ISSN 1070-3284, Russian Journal of Coordination Chemistry, 2021, Vol. 47, No. 4, pp. 296–305. © Pleiades Publishing, Ltd., 2021.

Two New 3D Metal-Organic Frameworks Constructed by Polycarboxylate and N-Donor Ligands: Crystal Structure, Photocatalytic Performances, and DFT Calculation

X. Y. Tan[a], J. Wang[a, *], C. Y. Rao[b], L. Lu[a], L. T. Wei[b], A. Q. Ma[b, **], and M. Muddassir[c]

[a] *School of Chemistry and Environmental Engineering, Sichuan University of Science & Engineering, Zigong, 64300 P.R. China*

[b] *Dongguan Key Laboratory of Drug Design and Formulation Technology, School of Pharmacy, Guangdong Medical University, Dongguan, 523808 P.R. China*

[c] *Department of Chemistry, College of Sciences, King Saud University, Riyadh, 11451 Saudi Arabia*

**e-mail: scwangjun2011@126.com*

***e-mail: maqandght@126.com*

Received May 28, 2020; revised June 26, 2020; accepted June 26, 2020

Abstract—Two new metal-organic frameworks, [Zn(Bdc)(Bip)·H_2O] (**I**) and {[$Cd_2(Btc)_2(H_2O)_2$](H_2Bib)·$6H_2O$} (**II**) (H_2Bdc = 1,3-benzenedicarboxylic acid, H_3Btc = 1,3,5-benzenetricarboxylic acid, Bib = 1,4-bis(2-methylimidazol-1'-yl)butane, Bip = 1,5-bis(2-methylimidazol-1-yl)pentane), have been successfully synthesized solvothermally and characterized by elemental analyses, UV–Vis spectroscopy, photocatalysis and single crystal X-ray diffraction (CIF files CCDC nos. 1982779 (**I**) and 1982780 (**II**). Complex **I** exhibits a 3-fold interpenetrating motif having dmp net with $\{6^5\cdot8\}$ topology, complex **II** possesses 3D anionic network comprising of 3,6-connected $\{4\cdot6^2\}_2\{4^2\cdot6^{10}\cdot8^3\}$ topology. These MOFs could be taken as photocatalysts for degrading the methyl violet (MV), in which indicate their effective photocatalytic behavior for the degradation of MV. In addition, the suggested photocatalytic mechanism through density of states plots for **I** and **II** was discussed.

Keywords: MOF, carboxylate, crystal structure, photocatalytic activity, density of states

DOI: 10.1134/S1070328421040072

INTRODUCTION

During the last two decades, rapidly expanding developing area of photocatalysis and adsorbent had been utilized to degrade and removal effectively the organic molecules, which are lethal contaminants existing in the industrial waste [1–6]. Such technique is considered to be as a green and environmental strategy because it decomposes the organic aromatic dyes without adding further contaminants in water [1]. Although variety of photocatalytic materials had been developed until now, many efforts had been devoted to explore new and efficient photocatalytic materials, including metal-organic frameworks (MOFs). MOFs possess unique 3D structural frameworks with semiconducting properties [7, 8]. Many investigations have manifested that combination of these mixed ligand methods based on the nitrogen donor and aromatic polycarboxylate ligands can be the effective pathway to construct diverse MOFs [9–12].

Recently, several MOFs have been synthesized and their capacity to degrade methyl violet (MV) has been explored [13, 14]. But despite their utility as the prudent photocatalysts for the photodecomposition of the aromatic dyes, the retention in crystallinity after photocatalysis and stability of MOFs are still a challenging aspect. Therefore, the rational selection of metal ions and ligands is of utmost importance to afford MOFs [15–20].

We continue to explore the direction of research in this field and plan to inspect the effect of angular dicarboxylate ligands in the formation of MOFs by tuning the auxiliary linkers and the metal centers. The selection of these N-donors is based on some peculiar coordination features these ligands display: (1) the 2-methylimidazol-1-yl group shows chelating coordination capacity and (2) such groups can freely twist around the $-CH_2-$ groups to meet the coordination requirements of the metal centers during self-assembly processes which therefore can fine tune the photophysical properties of resulting MOFs [21–23]. Based on the above consideration, by introducing different carboxylate ligands such as 1, 3-benzenedicarboxylic acid (H_2Bdc) and 1,3,5-benzenetricarboxylic acid (H_3Btc) into the Cd(II)/Zn-bis(2-methylimidazol-1-yl) system, two new 3D MOFs are reported herein. Apart from the syntheses and structural characteriza-

tion of these MOFs, they have been taken as the photocatalysts for the efficient photodegradation of an aromatic MV. The results of these investigations are presented herewith.

EXPERIMENTAL

Materials and methods. All reagents used for the syntheses were available commercially and have been used without further purification. The powder X-ray diffraction (PXRD) data collection for the MOFs were done on Bruker ADVANCE X-ray diffractometer which was equipped with CuK_α radiation (λ = 1.5418 Å) at 50 kV, 20 mA with a scanning rate of 6°/min and a step size of 0.02°. The UV–Vis spectra of solution samples were obtained on a UV-9000S UV–Vis spectrophotometer (METASH, China).

Synthesis of [Zn(Bdc)(Bip)·H_2O] (I). A mixture of Bdc (0.10 mmol, 0.017 g), Bip (0.10 mmol, 0.022 g), $Zn(NO_3)_2{\cdot}6H_2O$ (0.15 mmol, 0.045 g) and 10 mL DMF–H_2O mixture (v/v = 1 : 1) was stirred for 30 min and then transferred and thereafter sealed in a 25 mL Teflon-lined reactor. The reactor was heated to 120°C for 72 h, and then cooled to room temperature with cooling rate of 5°C/h. After cooling down to room temperature the colorless block crystals of **I** were obtained in 59% yield based on zinc.

For $C_{21}H_{26}N_4O_5Zn$ (**I**)

Anal. calcd., %	C, 52.57	H, 5.46	N, 11.68
Found, %	C, 52.68	H, 5.49	N, 11.72

IR (KBr; ν, cm^{-1}): 3490 v, 3148 w, 2926 w, 1602 m, 1486 m, 1371 s, 1288 m, 1141 m, 1085 m, 813 s, 745 s, 570 m.

Synthesis of {[Cd_2(Btc)$_2$(H_2O)$_2$](H_2Bib)·6H_2O} (II). The synthesis procedure of **II** was analogous to that of **I**, except that $Zn(NO_3)_2{\cdot}6H_2O$, Bdc and Bib were replaced by $Cd(NO_3)_2{\cdot}6H_2O$ (0.10 mmol), H_3Btc (0.10 mmol) and Bip (0.10 mmol). Colorless block crystals of **II** were obtained in 71% yield based on cadmium.

For $C_{15}H_{21}N_2O_{10}Cd$ (**II**)

Anal. calcd., %	C, 35.91	H, 4.22	N, 5.58
Found, %	C, 36.02	H, 4.19	N, 5.35

IR (KBr; ν, cm^{-1}): 3364 v, 2921 w, 1616 m, 1546 m, 1420 m, 1364 s, 1113 m, 947 s, 772 m, 716 s, 528 w.

X-ray crystallography. The single crystal X-ray diffraction data collection was executed on Bruker SMART APEX diffractometer having graphite monochromated MoK_α radiation (λ = 0.71073 Å) at T = 273 K by using an ω-scan technique. The structure of the MOFs were solved by using direct method (SHLEX-2014) and refined using the full-matrix least-squares procedure based on F^2 (SHELXL-2014) [24]. All the hydrogen atoms were generated geometrically and refined isotropically using a riding model. All non-hydrogen atoms were refined with anisotropic displacement parameters. The pertinent crystallographic details and selected geometrical parameters for **I** and **II** are listed in Table 1 and Table 2, respectively.

Supplementary material for structures has been deposited with the Cambridge Crystallographic Data Centre (CCDC nos. 1982779 (**I**) and 1982780 (**II**); deposit@ccdc.cam.ac.uk or http://www.ccdc.cam.ac.uk).

Photocatalytic method. The sample of the MOF **I**/**II** (40 mg) was dispersed in 50 mL aqueous solution of methyl violet (10 mg/L) in dark under stirring for 30 min to establish the adsorption-desorption equilibrium. Thereafter, the photocatalytic degradation of MV was performed in XPA-7 type photochemical reactor having 100 W mercury lamp (mean wavelength 365 nm) with light intensity of 12.7 mW/cm^2 at quartz tube positions. During photodecomposition experiments, aliquots of 3.0 mL were taken out.

Computational details. The possible photocatalytic mechanism associated with the **I** and **II** has been to be explicated using density of states (DOS) calculations. To obtain DOS plots the smallest unit of MOFs was geometry optimized using the B3LYP functional [25] using 6-31G** basis set for all the atoms except metal centers. For Zn(II) and Cd(II) metal centers CEP-121G basis set was employed. All the calculations were performed using Gaussian 09 program [26]. GaussSum 3.0 was used to obtain DOS and partial DOS (pDOS) plots [27].

RESULTS AND DISCUSSION

The asymmetric unit of the molecule comprises of one Zn(II) center, one Bip ligand, one free water molecule and one Bdc^{2-} ligand in **I** (Fig. 1a, Table 1). The immediate geometry around the Zn(1) center can be described as distorted tetrahedral where the tetrahedral positions are occupied by two nitrogen centers of two different Bip ligands (Zn(1)–N(4) 1.988(5) and Zn(1)–N(4) 2.020(5) Å) and two oxygen centers from two different Bdc^{2-} anions (Zn(1)–O 1.935(5)–1.942(4) Å) (Table 2). A peculiar structural feature of **I** is the existence of two types of helical chains both running along the *b* direction. The Bdc^{2-} also adopts monodentate bridging coordination mode and bridging Zn(II) centers to shape one left-handed helical chains $[Zn(Bdc)]_n$ along the *b* axis with a pitch of 10.367 Å (Fig. 1b, Scheme S1), while the adjacent chains are linked together by Bib ligands. Meanwhile, each Bib adopts the trans-conformation to bridge Zn^{2+} ions into 1D right-helical chain $[Zn(Bip)]_n$ (Fig. 1c). The left-handed helical chains $[Zn(Bdc)]_n$ are further connected by the chains $[Zn(Bip)]_n$ to gen-

Table 1. Crystallographic data and structure refinement details for complexes **I** and **II**

Parameter	Value	
	I	**II**
Formula weight	479.85	501.74
Crystal system	Orthorhombic	Monoclinic
Space group	*Pca*21	*P*21/*n*
Crystal color	Colorless	Colorless
a, Å	21.2001(18)	10.2857(14)
b, Å	10.0682(9)	13.8579(19)
c, Å	10.3892(9)	13.2746(19)
α, deg	90	90
β, deg	90	90.001(1)
γ, deg	90	90
V, Å^3	2217.5(3)	1892.1(5)
Z	4	4
ρ_{calcd}, g/cm^3	1.437	1.761
μ, mm^{-1}	1.147	1.211
F(000)	1000	1012
θ Range, deg	2.7–27.5	2.9–27.5
Reflection collected	4781	4243
Independent reflections (R_{int})	0.039	0.035
Reflections with $I > 2\sigma(I)$	3648	3565
Number of parameters	283	254
R_1, wR_2 ($I > 2\sigma(I)$)*	0.0461, 0.1271	0.0428, 0.1108
R_1, wR_2 (all data)**	0.0681, 0.1422	0.0522, 0.1188

* $R = \Sigma(F_o - F_c)/\Sigma(F_o)$, ** $wR_2 = \{\Sigma[w(F_o^2 - F_c^2)^2]/\Sigma(F_o^2)^2\}^{1/2}$.

erate a 3D structure (Fig. 1d) [28]. The potential voids are large enough to allow two independent identical networks, leading to a 3D 2-fold interpenetrating architecture, and exhibit a 4-connected dmp net with the point symbol of $\{6^5\cdot8\}$ (Fig. 1e).

When the Bdc^{2-} ligand and Zn(II) were replaced with H_3Btc and Cd(II), a new 3D MOF (II) was synthesized. It was found that **II** shows two equivalent Cd(II) centers are connected by two μ_2,η^2-carboxylate groups from adjacent Btc to form a dinuclear unit (Figs. 2a, 2b, Fig. S1 and Scheme S1). Furthermore, μ_2,η^2-bridging and chelating carboxylate from Btc bridge dinuclear unit to yield a 1D chain. Further linkage of these 1D chains by monodentate carboxylate group gives rise to a 3D anionic motif comprising of 1D channels (Fig. 1d, Fig. S2). The intermolecular O–H···O hydrogen bonding interactions operating between lattice water molecules (O(8), O(9) and O(10)) and the coordinated water molecule further stabilize this structure (Figs. 2f, S3) and this framework is similar to the previously reported structure [29–32]. From the topological viewpoint, the interconnection of dinuclear unit and Btc generates a 3,6-connected topology with the Schläfli symbol $\{4\cdot6^2\}_2\{4^2\cdot6^{10}\cdot8^3\}$ (Fig. 2d).

To estimate the behavior of **I** and **II** as photocatalysts for the degrading the aromatic methyl violet (MV) had been selected as a model aromatic dye contaminant commonly existing in the waste water discharge. The variation in the intensity of the peculiar UV–Vis absorption bands of MV with time in the presence of both the MOFs used as the photocatalysts are

Table 2. Selected bond distances (Å) and angles (deg) for **I** and **II***

Bond	*d*, Å	Bond	*d*, Å
		I	
Zn(1)–O(1)	1.942(4)	Zn(1)–N(1)	2.020(5)
Zn(1)–O(3)$^{\#1}$	1.936(5)	Zn(1)–N(4)$^{\#2}$	1.989(4)
		II	
Cd(01)–O(1)	2.273(4)	Cd(01)–O(5)	2.360(4)
Cd(01)–O(3)$^{\#1}$	2.363(3)	Cd(01)–O(7)$^{\#1}$	2.634(5)
Cd(01)–O(2)$^{\#2}$	2.452(3)	Cd(01)–O(6)$^{\#2}$	2.349(4)
Cd(01)–O(4)$^{\#3}$	2.268(4)		
Angle	ω, deg	Angle	ω, deg
		I	
O(1)Zn(1)N(1)	98.1(2)	O(1)Zn(1)O(3)$^{\#1}$	106.0(2)
O(1)Zn(1)N(4)$^{\#2}$	115.30(18)	O(3)$^{\#1}$Zn(1)N(1)	111.8(2)
N(1)Zn(1)N(4)$^{\#2}$	107.3(2)	O(3)$^{\#1}$Zn(1)N(4)$^{\#2}$	116.8(3)
		II	
O(1)Cd(01)O(5)	80.10(14)	O(1)Cd(01)O(3)$^{\#1}$	82.07(13)
O(1)Cd(01)O(7)$^{\#1}$	94.08(14)	O(1)Cd(01)O(6)$^{\#2}$	144.24(12)
O(1)Cd(01)O(4)$^{\#3}$	126.96(12)	O(3)$^{\#1}$Cd(01)O(5)	146.38(12)
O(5)Cd(01)O(7)$^{\#1}$	159.64(12)	O(2)$^{\#2}$Cd(01)O(5)	85.65(10)
O(5)Cd(01)O(6)$^{\#2}$	92.92(13)	O(4)$^{\#3}$Cd(01)O(5)	82.62(14)
O(2)$^{\#2}$Cd(01)O(3)$^{\#1}$	123.78(10)	O(3)$^{\#1}$Cd(01)O(6)$^{\#2}$	116.76(14)
O(3)$^{\#1}$Cd(01)O(4)$^{\#3}$	83.56(12)	O(2)$^{\#3}$Cd(01)O(7)$^{\#1}$	74.33(11)

* Symmetry codes: $^{\#1}$ $1-x, 2-y, -1/2+z$; $^{\#2}$ $1/2-x, 1+y, -1/2+z$ (**I**). $^{\#1}$ $3/2-x, 1/2+y, 1/2-z$; $^{\#2}$ $1-x, 1-y, -z$; $^{\#3}$ $2-x, 1-y, -z$ (**II**).

illustrated in Figs. 3a, 3b. As indicated in Figs. 3a, 3b, the intensity of the UV–Vis absorption band declines significantly during the irradiation period of 40 min. This suggests that both the MOFs are capable of photocatalysts for photodegrading the MV. In addition, the variation in the concentrations of MV (*c*) vs. reaction time (τ) in the presence of **I** and **II** has been measured (Figs. 3c, 3d). These results demonstrate the noticeable photocatalytic behavior of both the MOFs to decompose the MV in water. Also this indicates that Zn(II) containing **I** offered relatively better photocatalytic property than the Cd(II) containing **II**. Further, the total the percentage photocatalytic decomposition of the MV under control experimental condition in the absence of the MOFs is merely 16%. In comparison to the control experiment the MOF based photocatalysts **I** and **II** displayed much improved MV decomposition (**I**: 69% and **II**: 66%). The photocatalytic activities of **I** and **II** were comparable with selected reported MOFs and inorganic materials (Table 3) [33–42]. Moreover, the photocatalytic results indicate that **I** may be good heterogeneous catalyst for the light-driven degradation of MV in water (Fig. 3c). The relatively better photocatalytic performance of **I** may be due to the distinct 3D framework constructed by Bib ligands and Bdc^{2-} ions to accelerate the electron and hole transfer process [1, 43].

Further, to calculate the degradation rate of MV in the presence of **I** and **II**, the reaction rate constants (*k*) were calculated by adopting the pseudo-first-order kinetic equation in accordance with the Langmuir Hinshelwood. The rate constants *k* calculated based on this equation were 0.02997 min^{-1} (R^2 = 0.99345 for **I**), 0.02842 min^{-1} (R^2 = 0.99196) for **II** (Fig. 3d).

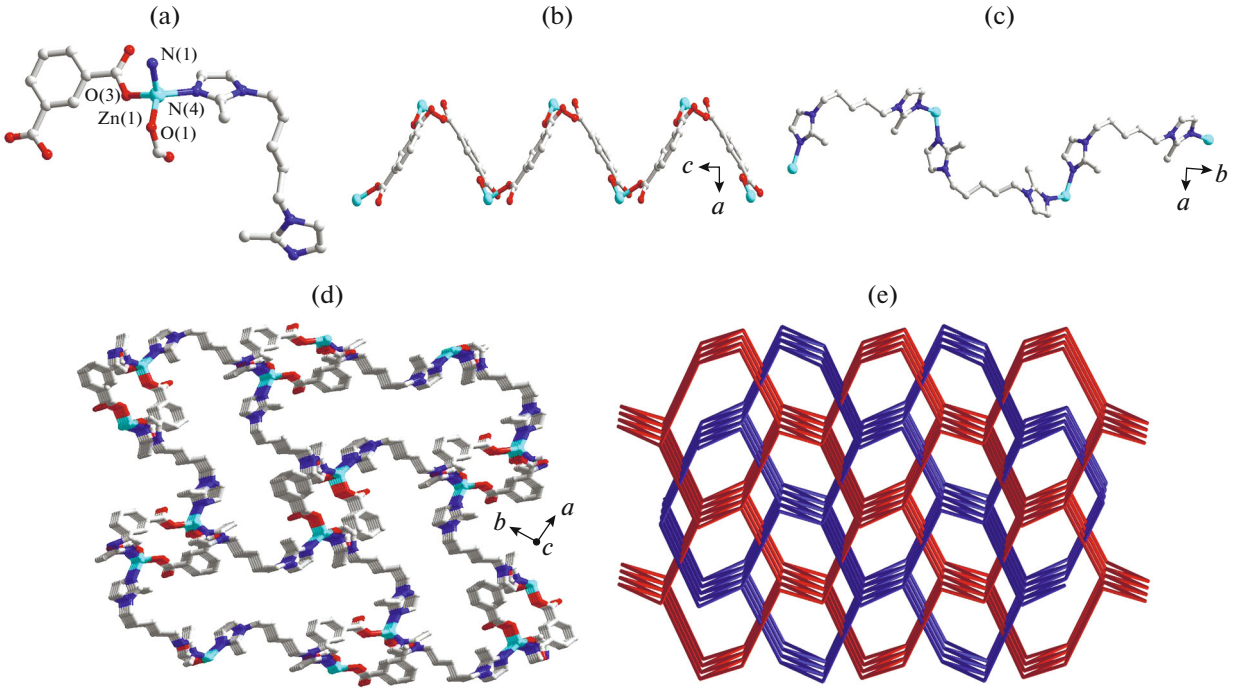

Fig. 1. Perspective view of the coordinated geometry around Zn(II) center in **I** (a); view of right-handed and left-handed helical chains in **I** (b) and (c), respectively; a single 3D network (d); topological representation of the 2-fold interpenetrating network of **I** (e).

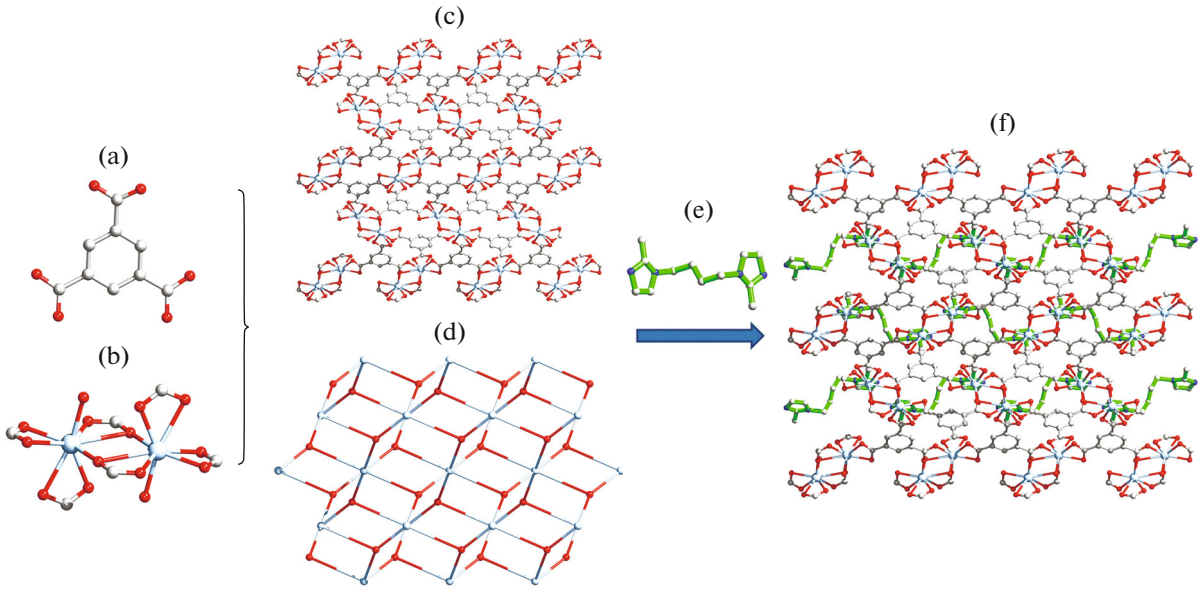

Fig. 2. The view of Btc^{3-} ligand (a); the two crystallographically equivalent Cd(II) centers in **II** (b); the 3D motif existing in **II** (c); perspective view of the (3,6)-connected topology with the symbol being $\{4\cdot6^2\}_2\{4^2\cdot6^{10}\cdot8^3\}$ (d); the view of Bib ligand (e); the free molecule of Bib located in the pores of **II** (f).

The pseudo-first-orderrate constants (k) and the correlation coefficients (R^2) are listed in Table 4.

To explore the possible mechanism and to check the nature of reactive species, which may explain the decomposition of MV. Then the degradation of MV was conducted using tertiary butyl alcohol (TBA), benzoquinone (BQ) and ammonium oxalate (AO) which take as ·OH, $O_2\cdot^-$ and h^+ radicals quenchers, respectively (Figs. 4a and 5a) [40]. The reactions performed in presence of these quenchers showed that

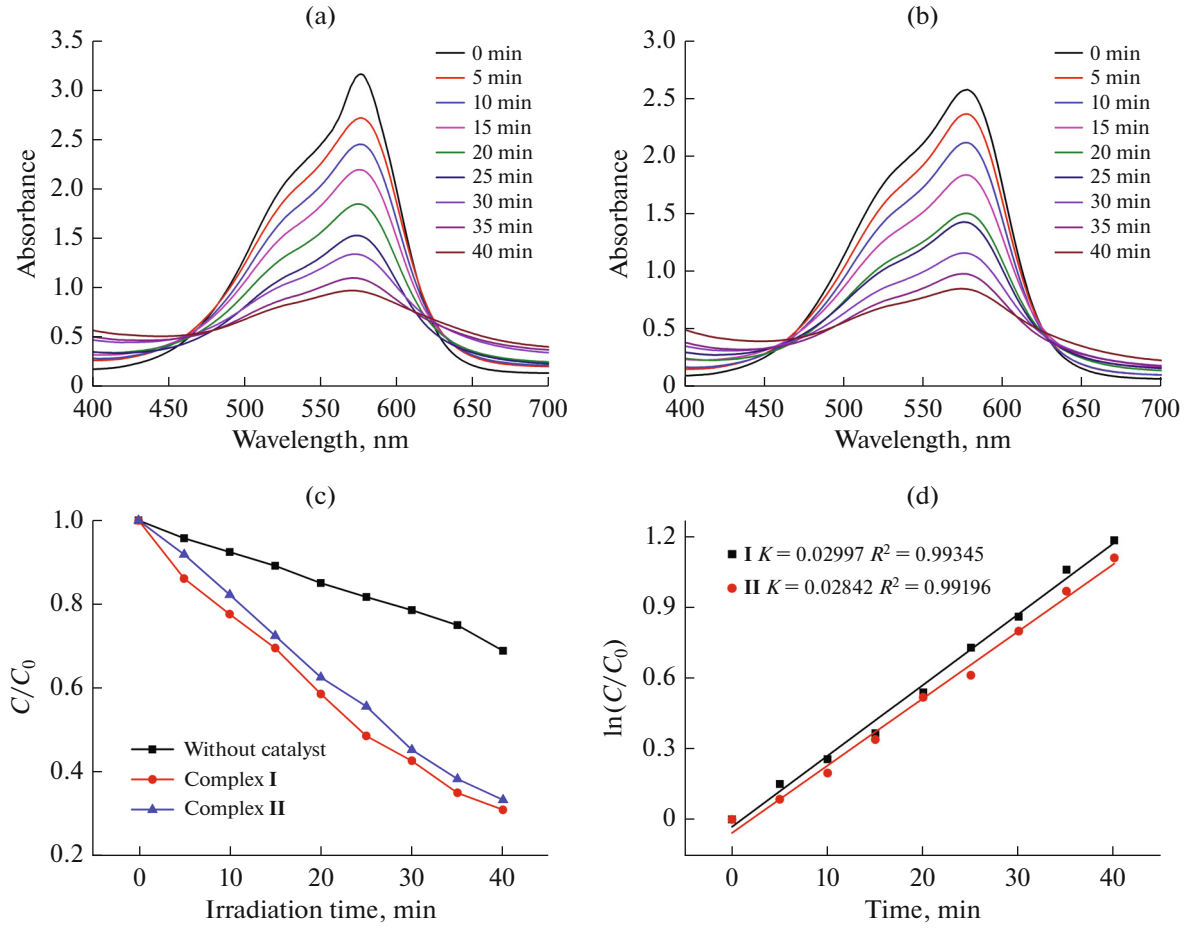

Fig. 3. Absorption intensity of the MV solutions in the presence of **I** and **II** (a) and (b), respectively; photocatalytic decomposition of MV solution under UV–Vis light irradiation with the use of **I** and **II** and the control experiment without any catalyst (c); linear-log plot as a function of visible light irradiation time in the presence of **I** and **II** (d).

Table 3. Performances of selected photocatalysts for the degradation of MV

Compound	Irradiation	Degradation efficiency, %	Reference
$[Zn_7(NDC)_{5.5}(\mu_4\text{-}OH)_3]$	UV	65	32
$[Cd(Pa)(Bip)(H_2O)]$	UV	61	33
$[Zn_2(Pa)_2(Bip)_2]$	UV	52	34
$[Zn_4(\mu_2\text{-}OH)_2(BDC)_3(Bip)_2]$	UV	82	35
[Cd(L)(HBpz)]	UV	59	36
[Zn(Bidpe)(Mpa)]	UV	91.1	37
[Cd(Bidpe)(Mpa)]	UV	39.2	38
$[Zn_{1.5}(Bidpe)_2(Smpa)(H_2O)]$	UV	39.1	38
[Cd(Bidpe)(Hmpa)]	UV	93.2	39
$[Zn_2(Fer)_2]$	UV	54	40
$[Cu_3(H_3Tpb)_2(Tpb)(Mo_4O_{12})]$	UV	95	41
$[Zn_3(Btc)_2(Bimmb)_{2.5}]$	UV	92.16	42
$[Co_2(BTC)(L)]$	UV	91	43
$Bi_6O_6(OH)_2(NO_3)$	UV	93	44
$CdFe_{12}O_{19}$	UV	62.27	45
I	UV–Vis	75	This work
II	UV–Vis	65	This work

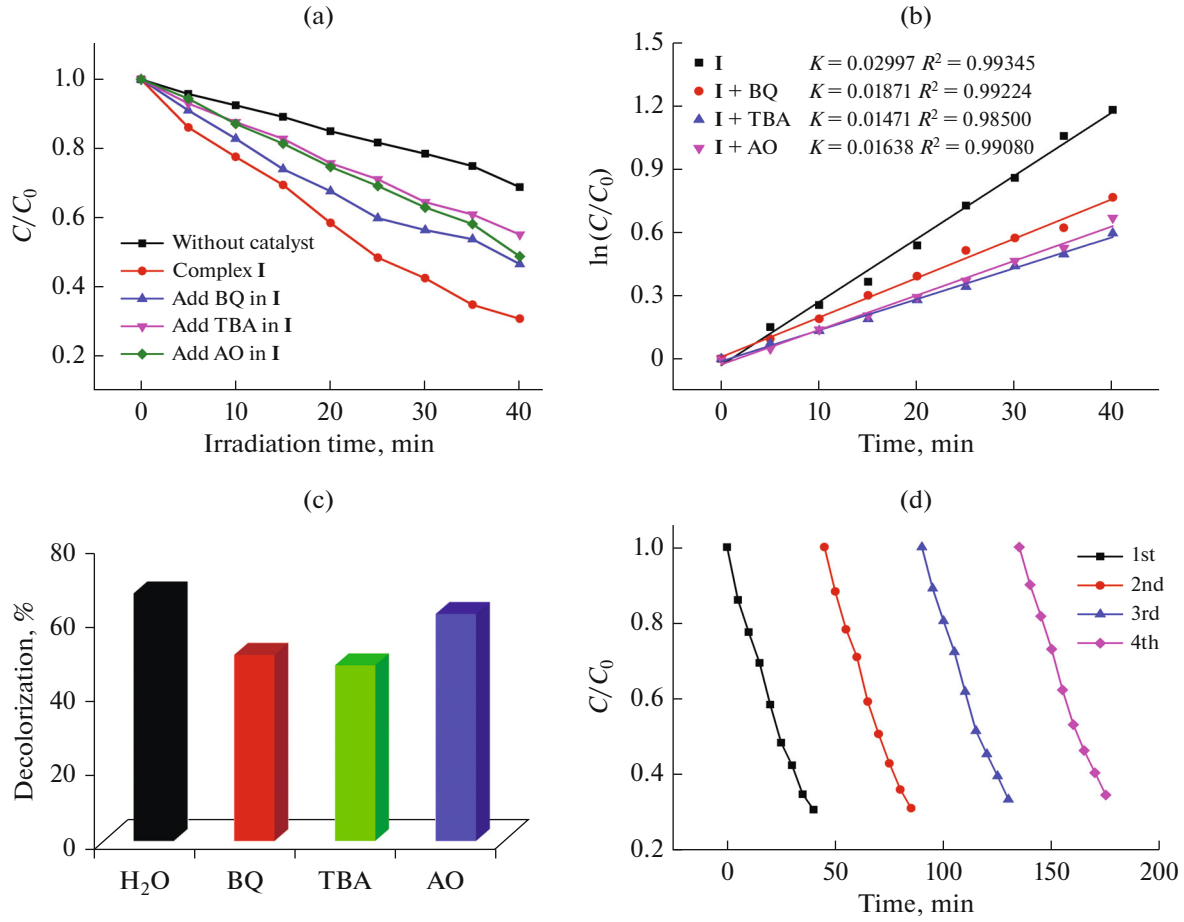

Fig. 4. Photocatalytic decomposition of MV solution under the use of **I** and different scavenger solutions (a) and (c); linear-log plot as irradiation time in the presence of **I** and different scavengers (b); cycling four runs feature **I** for degradation of MV (d).

TBA can decrease the photodegradation of MV in **I** and **II** (Figs. 4b, 4c, 5b, 5c). The quenching experiments indicated that the *k* values for the decomposition of MV in presence of **I** and **II** were found to decrease from 0.02997 to 0.01471 min^{-1} for **I**, 0.02842 to 0.01441 min^{-1} for **II** in the presence of TBA. Therefore, the results suggest that the photodegradation of MV by the photocatalysts **I** and **II** is dominated by ·OH system [44–46].

Table 4. The kinetic parameters of photodegradation reactions of MV in presence of **I** and **II**

Material	MV	
	k, min^{-1}	R^2
I	0.02997	0.99345
I + BQ	0.01871	0.99224
I + TBA	0.01471	0.99500
I + AO	0.01638	0.99080
II	0.02842	0.99196
II + BQ	0.01553	0.99347
II + TBA	0.01441	0.99064
II + AO	0.02280	0.98505

Further to assess the stability of these photocatalysts, the MOFs **I** and **II** were recovered from the reaction mixture by filtration and the obtained MOF based materials were found to be stable as both the recovered MOFs displayed similar PXRD pattern as can be obtained from the as-synthesized pristine MOFs (Figs. S4 and S5). Also, these recovered MOFs offered photodegradation of MV for another four catalytic cycles and in total four catalytic cycles (Figs. 4d and 5d) and the degradation rates of MV in presence of MOFs **I** and **II** exhibited no significant decrease, which further suggests that the photocatalytic activities of both the MOFs good reproducibility.

As an attempt to establish the plausible mechanism adopted for **I** and **II** assisted photodegradation of MV, the band structure calculations were executed using density functional theory (DFT). Hence, to assess the band structure of both the MOFs, DOS and pDOS plots have been constructed (Figs. 6a, 6b). The plots display that the valence band in **I** and **II** has major

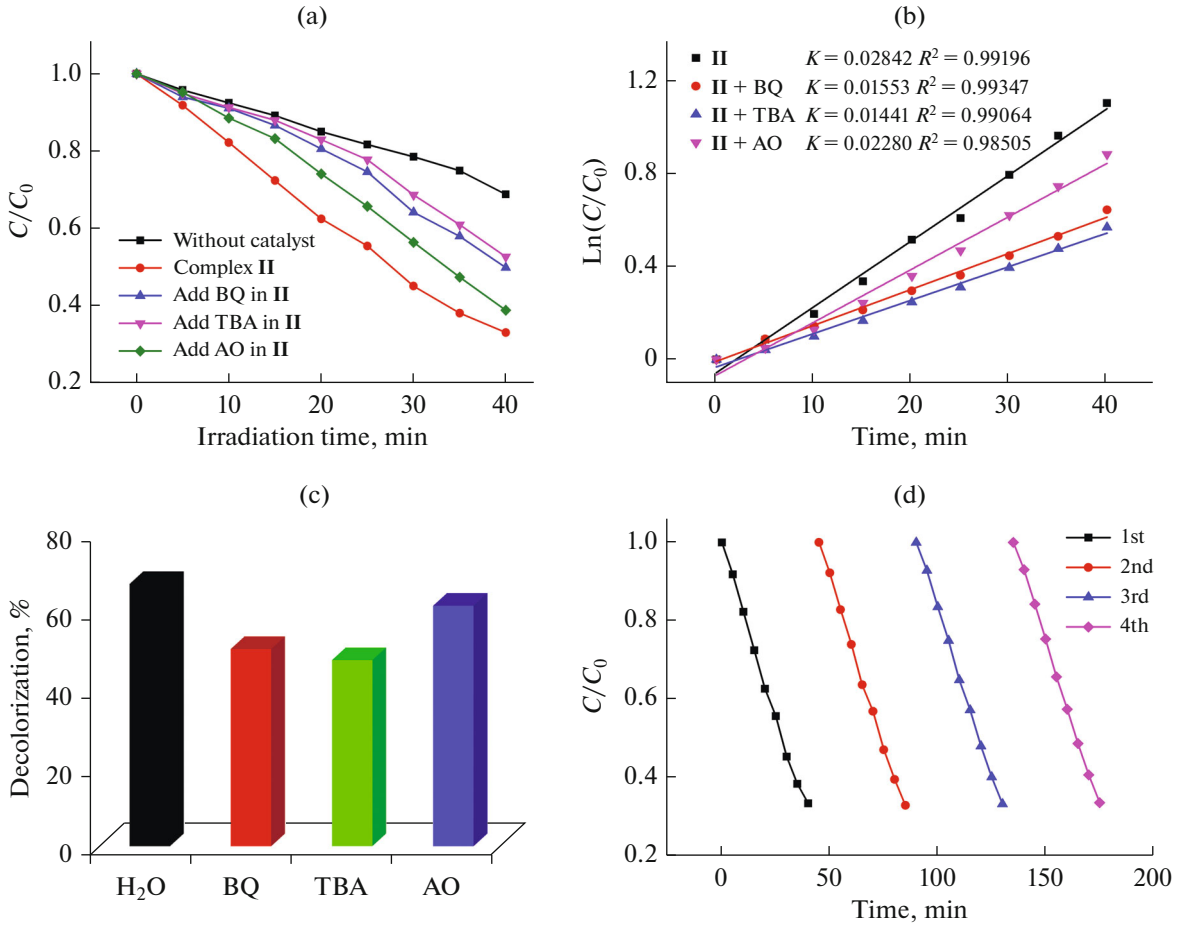

Fig. 5. Photocatalytic decomposition of MV solution under UV–Vis light irradiation with the use of **II** and different scavenger solutions (a); linear-log plot as a function of visible light irradiation time in the presence of **II** and different scavengers (b); photodegradation of the MV solution over **II** in the different scavenger solutions (c); cycling four runs of the photocatalytic degradation of MV for **II** (d).

contribution from aromatic carbons and carboxylate oxygens, and also from nitrogen of Bip ligand in **I** and meagre contribution from zinc and cadmium centres in **I** and **II**, respectively. Hence, on the basis of DOS and pDOS plots it can be inferred that electronic transitions in the MOFs **I** and **II** are of the ligand-to-ligand type taking place from one aromatic center to another aromatic center. The variation in energy band gap in both the MOFs is the most plausible reason for the differences in their photocatalytic performances. Also, in the case of **II**, the nitrogen donor ligand H_2Bip is not coordinated to the Cd(II) center and hence is not playing a decisive role in the framework generation as well as the electronic communication in this MOF. This may be also be another reason due to which the MOF **II** is offering relatively inferior photocatalytic properties [47].

In summary, two new d^{10}-metal based MOFs having Zn(II) and Cd(II) centers have been synthesized which possess entirely different topologies. These MOFs further have been used as the photocatalysts for the photodecomposition of methyl violet (MV) under ultraviolet irradiation and offered different photocatalytic properties. The differences in photocatalytic properties had been attributed to the differences in the band gap and existence of distinct 3D framework in Zn(II) based MOF to accelerate the electron and hole transfer process.

FUNDING

The authors acknowledge financial assistance from Sichuan University of Science and Engineering (nos. 2019RC21), the Project of Zigong Science and Technology (nos. 2018YYJC01 and 2019YYJC06), the Student's Platform for Innovation and Entrepreneurship Training Program (cx2019013), and Special Funds for Scientific Technological Innovation of Undergraduates in Guangdong Province (pdjh2020b0267 and pdjh2020b0265). Dr. Mohd. Muddassir is grateful Researchers Supporting Project (RSP-2019/141), King Saud University, Riyadh, Saudi Arabia for financial assistance.

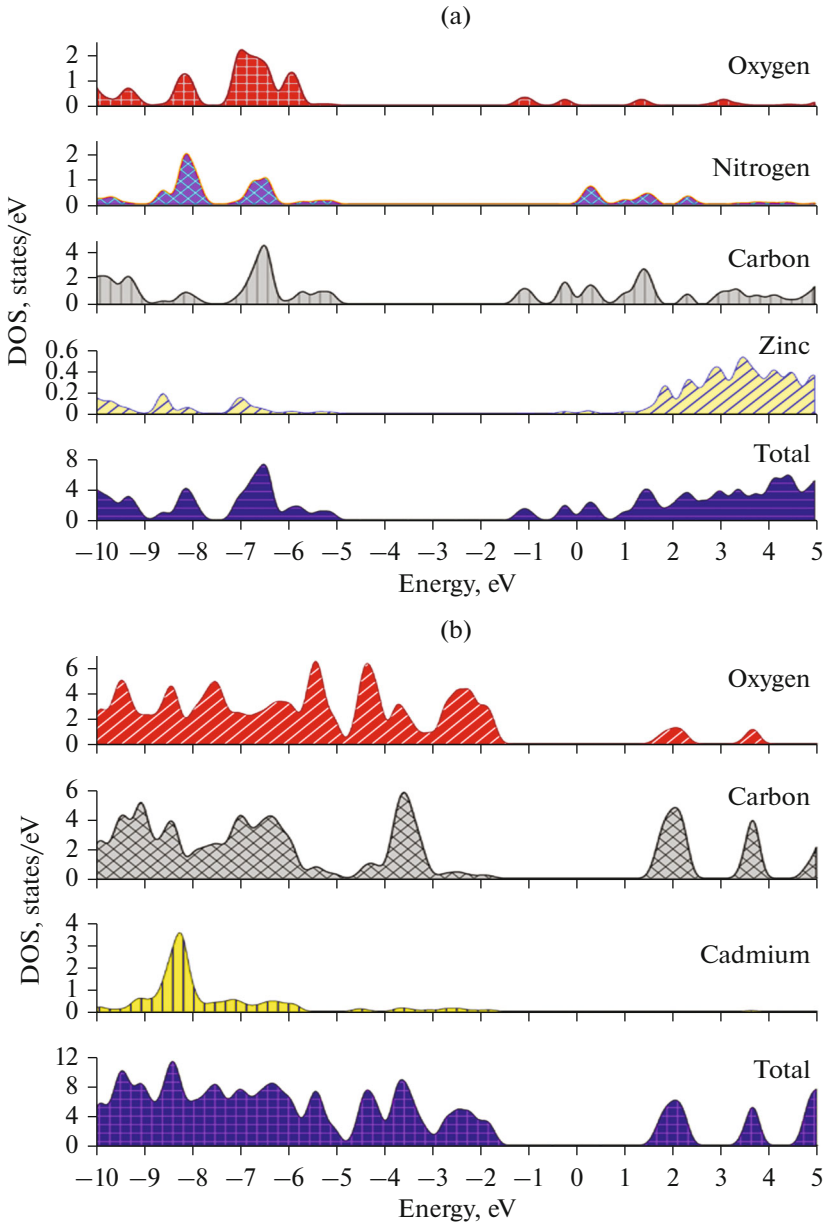

Fig. 6. DOS and partial DOS plots for **I** and **II** (a) and (b), respectively.

CONFLICT OF INTEREST

The authors declare that they have no conflicts of interest.

SUPPLEMENTARY INFORMATION

The online version contains supplementary material available at https://doi.org/10.1134/S1070328421040072.

REFERENCES

1. Li, H.X., Zhang, X., Huo, Y.Y., et al., *Environ. Sci. Technol.*, 2007, vol. 41, p. 4410.
2. Li, M., Liu, L., Zhang, L., et al., *CrystEngComm*, 2014, vol. 16, p. 6408.
3. Yu, Z.T., Liao, Z.L., Jiang, Y.S., et al., *Chem. Eur. J.*, 2005, vol. 11, p. 2642.
4. Pan, Y., Ding, Q.J., Li, B.H., et al., *Chemosphere*, 2021, vol. 263, p. 128101.
5. Liu, W.C., Shen, X., and Han, Y.Y., *Chemosphere*, 2019, vol. 215, p. 524.
6. Ma, A.Q., Wu, J., Han, Y.T., et al., *Dalton Trans.*, 2018, vol. 47, p. 9627.
7. Liu, K.G., Rouhani, F., Gao, X.M., et al., *Catal. Sci. Technol.*, 2020, vol. 10, p. 757.
8. Wu, X.R., Shen, X., Fan, S.R., et al., *RSC Adv.*, 2018, vol. 8, p. 23529.
9. Hu, J.S., Shang, Y.J., Yao, X.Q., et al., *Cryst. Growth Des.*, 2010, vol. 10, p. 4135.

10. Hu, M.-L., Mohammad, Y.M., and Morsali, A., *Coord. Chem. Rev.*, 2019, vol. 387, p. 415.
11. Hu, M.-L., Razavi, S.A., Piroozzadeh, M., et al., *Inorg. Chem. Front.*, 2020, vol. 7, p. 1598.
12. Liu, J.-Q., Luo, Z.-D., Pan, Y., et al., *Coord. Chem. Rev.*, 2020, vol. 406, p. 213245.
13. Wu, Y., Wu, J., Luo, Z.D., et al., *RSC Adv.*, 2017, vol. 7, p. 10415.
14. Wu, Y., Lu, L., Feng, J.S., et al., *J. Solid State. Chem.*, 2017, vol. 245, p. 213.
15. Liu, J., Wang, E., Luo, Z., et al., *Inorg. Chem.*, 2017, vol. 56, p. 10215.
16. Wang, J., Wu, X.R., Liu, J.Q., et al., *CrystEngComm*, 2017, vol. 19, p. 3519.
17. Wang, J., Bai, C., Hu, H.M., et al., *J. Solid State. Chem.*, 2017, vol. 249, p. 87.
18. Lu, L., Wang, J., Xie, B., et al., *New. J. Chem.*, 2017, vol. 41, p. 3537.
19. Pan, Y., Liu, W.C., Liu, D., et al., *Inorg. Chem.* Commun., 2019, vol. 100, p. 92.
20. Chang, X.H., Zhao, Y., Han, M.L., et al., *CrystEngComm*, 2014, vol. 16, p. 6417.
21. Yang, E.C., Liu, Z.Y., Shi, X.J., et al., *Inorg. Chem.*, 2010, vol. 49, p. 7969.
22. Xu, J., Pan, Z.R., Wang, T.W., et al., *CrystEngComm*, 2010, vol. 12, p. 612.
23. Huang, S.L., Lin, Y.J., Andy Hor, T.S., et al., *J. Am. Chem. Soc.*, 2013, vol. 135, p. 8125
24. Sheldrick, G.M., *Acta Crystallogr., Sect. A: Found. Adv.*, 2015, vol. 7, p. 3.
25. Becke, A.D., *J. Chem. Phys.*, 1993, vol. 98, p. 5648.
26. Lee, C.T., Yang, W.T., and Parr, R.G., *Phys. Rev. B: Condens. Matter Mater. Phys.*, 1998, vol. 37, p. 785.
27. Frisch, M.J., Trucks, G.W., Schlegel, H.B., et al., *Gaussian 09, Revision B.01*, Wallingford: Gaussian, Inc., 2009.
28. Chang, X.H., Qin, J.H., Han, M.L., et al., *CrystEngComm*, 2014, vol. 16, p. 870.
29. He, T., Yan, N., Yuan, W.Z., et al., *Polyhedron*, 2016, vol. 118, p. 118.
30. Zhou, H.F., He, T., Yue, K.F., et al., *Cryst. Growth Des.*, 2016, vol. 16, p. 3961.
31. Li, X.J., Sun, X.F., Li, X.X., et al., *Cryst. Growth Des.*, 2015, vol. 15, p. 4543.
32. Ding, Q., Pan, Y., Luo, Y., et al., *ACS. Omega*, 2019, vol. 4, p. 10775.
33. Wang, J., Lu, L., He, J.R., et al., *J. Mol. Struct.*, 2019, vol. 1182, p. 79.
34. Lu, L., He, J., Wang, J., et al., *J. Mol. Struct.*, 2019, vol. 1179, p. 612.
35. Cai, S.L., Lu, L., Wu, W.P., et al., *Inorg. Chim. Acta*, 2019, vol. 484, p. 291.
36. Zong, Z., Fan, C., Bi, C., et al., *J. Solid State. Chem.*, 2019, vol. 270, p. 651.
37. Zhou, E.H., Li, B.H., Chen, W.X., et al., *J. Mol. Struct.*, 2017, vol. 1149, p. 352.
38. Jin, J.C., Wu, X.R., Luo, Z.D., et al., *CrystEngComm*, 2017, vol. 19, p. 4368.
39. Zhang, X.T., Fan, L.M., Zhang, W., et al., *Dalton Trans.*, 2013, vol. 42, p. 16562.
40. Yu, Y.F., Zong, Z., Fan, C.B., et al., *Inorg. Nano-Metal. Chem.*, 2019, vol. 49, p. 455.
41. Li, A.L., Hao, Z.C., Han, C., et al., *Appl. Organomet. Chem.*, 2020, vol. 34, p. e5313.
42. Zheng, M., Han, Q.F., Jia, X.M., et al., *Mat. Sci. Semicon. Proc.*, 2019, vol. 101, p. 183.
43. Du, P., Yang, Y., Yang, J., et al., *CrystEngComm*, 2013, vol. 15, p. 6986.
44. Yuan, F., Yuan, C.M., Zhou, C.S., et al., *CrystEngComm*, 2019, vol. 21, p. 6558.
45. Li, Y., Niu, J., Yin, L., et al., *J. Environ. Sci.*, 2011, vol. 23, p. 1911.
46. Wang, C.C., Li, J.R., Lv, X.L., et al., *Energy Environ. Sci.*, 2014, vol. 7, p. 2831.
47. Sinha, T. and Ahmaruzzaman, M., *Photochem. Photobiol. Sci.*, 2016, vol. 15, p. 1272.